

Early stage of crystallization of $(\text{Zr}_{1-x}\text{Hf}_x)_{62}\text{Ni}_{38}$ metallic glasses

Robert Schulz,* V. Matijasevic, and W. L. Johnson,

W. M. Keck Laboratory of Engineering Materials, California Institute of Technology, Pasadena, California 91125

(Received 4 June 1984)

This paper reports a directly observable correlation between the chemical short-range order and the electrical resistivity in metallic glasses. The phase transition corresponding to the first exotherm observed in a differential-scanning-calorimetry (DSC) scan on $(\text{Zr}_{1-x}\text{Hf}_x)_{62}\text{Ni}_{38}$ is peculiar in a sense that, contrary to usual metallic glasses, this transition is associated with an increase in electrical resistivity, and x-ray diffraction measurements taken just after the DSC peak shows only the broad diffuse band characteristic of the glassy phase. Electrical resistivity, differential scanning calorimetry, low-temperature superconducting measurements, high-angle x-ray diffraction, transmission electron microscopy, and Mössbauer spectroscopy are used to study this transition in detail.

I. INTRODUCTION

$(\text{Zr}_{1-x}\text{Hf}_x)_{62}\text{Ni}_{38}$ represents an attractive system in the field of metallic glasses for many reasons. First, it can be made amorphous over a very wide range of composition,¹ and, contrary to the better-known Cu-Zr system, it is more stable and not as sensitive to oxygen contamination. Second, this glass is probably the ideal candidate for the isomorphic substitution technique,² which consists of gradually replacing Zr by Hf in the amorphous matrix and using the different x-ray patterns to deconvolute the data into partial pair-distribution functions of the different constituent elements, Zr-Zr, Zr-Ni and Ni-Ni. This technique is based on the assumption that we can replace Zr by Hf without influencing the structure of the glass. In fact, Zr and Hf are similar in many aspects: they form a continuous series of solid solution, and they have similar Goldschmidt radii, electronegativity, etc. A study of the stability and the crystallization process of this system for different [Zr]/[Hf] ratios constitutes, then, a good test for the validity of this technique.

Buschow *et al.*³ were the first to observe the peculiar behavior associated with the first-differential-scanning-calorimetry (DSC) peak in Zr-Ni and Hf-Ni systems near 38 at. % Ni. Similar observations were reported recently by Altounian *et al.*¹ on the same system. The former authors suggest that the first transition in those amorphous alloys is a transition within the amorphous state and is comprised mainly of short-range atomic rearrangement. Dong *et al.*,⁴ on the other hand, claim, from x-ray-diffraction analysis, that for this composition the first exotherm arises from the crystallization of NiZr_2 and, the second, from crystallization of NiZr from the nickel-enriched glass. Summarizing the results of several authors^{1,4,5} on $\text{Zr}_x\text{Ni}_{1-x}$, we conclude that for $x > 66$ (up to 78) a single sharp exotherm arises from the simultaneous formation of the equilibrium phases α -Zr and NiZr_2 . For $60 < x < 66$ we observed two distinct exotherms, which, for $x > 62-63$, can be identified as crystallization of first NiZr_2 and then NiZr . For $x < 60$ (down to 50) initial crystallization of NiZr followed almost instantaneously by

the crystallization of NiZr_2 from the Zr-enriched glass explains the asymmetric single DSC peak with a shoulder at high temperature observed in this range. Between $x = 60$ and $62-63$ the nature of the first exotherm changes from crystallization of NiZr to crystallization of NiZr_2 , and it is in this range that the high-angle x-ray pattern remains broad after the exotherm without any resolvable Bragg peaks. It is the purpose of this paper to study this peculiar transition in this range of concentration.

II. EXPERIMENT

The ingots were prepared by rf-induction-melting the appropriate amount of each constituent on a silver boat in an argon atmosphere. They were melted several times to ensure homogeneity. Glassy ribbons typically $30 \mu\text{m}$ thick, 2 mm wide, and several feet long were prepared by melt-spinning. They were examined by high-angle x-ray diffraction using $\text{Cu K}\alpha$ radiation. Only the samples showing a broad band characteristic of amorphous samples were kept for further study. For each composition, all measurements were done on the same ribbon to eliminate fluctuations in the free-volume content. The electrical resistivity was measured using a four-point dc method with pressure contact. The probe is free to move on a vertical axis inside a quartz tube, which goes through a furnace before being fixed at the top of a Dewar. The system can achieve very fast heating or cooling rates. Other details are described in Ref. 6. The DSC traces were obtained using a Perkin-Elmer DSC-1 under argon atmosphere at a heating rate of $20^\circ\text{C}/\text{min}$. Superconductivity down to around 1.6 K was studied through changes in the electrical resistance. The critical field was determined by plotting the resistance of the sample as a function of the magnetic field at a constant temperature maintained using a pressure-control valve over the He bath. The temperature was calculated using the vapor pressure of the helium. Samples for x-ray diffraction were prepared by stacking three layers of ribbons together with Duco[®] cement on a glass slide. The data were obtained in the reflection geometry on a Norelco scanning goniometer using

Mo $K\alpha$ radiation and a focusing LiF monochromator. The details for data correction and radial-distribution-function (RDF) calculations were described elsewhere.⁷ For transmission electron microscopy the specimens were thinned by jet-polishing using 80 vol % methanol and 20 vol % perchloric acid at -15°C . Samples for Mössbauer spectroscopy were prepared by introducing 0.2 at. % enriched ^{57}Fe in Zr-Ni as a probe element. The experiments were performed at room temperature on foils obtained by the "piston-and-anvil" technique. The source used was $^{57}\text{Co}(\text{Rh})$ and the experiments were done in the constant-acceleration mode.

III. RESULTS AND DISCUSSION

Figure 1 shows the DSC traces and the changes in resistance as we heat the samples through the crystallization temperature at a rate of 15 K/min. The DSC data were corrected for the difference in heating rate. Table I gives the temperatures corresponding to the onset of the two exotherms and the corresponding relative changes in electrical resistance for each transition. We see in Table I that Hf increases the stability of the glass by moving the peak's position to higher temperatures. Generally, the resistance decreases upon crystallization since the crystalline state has much greater atomic order. In our case, however, the first transition is accompanied by an increase of resistivity by roughly the same amount in all three alloys. An increase of resistivity upon crystallization has also been seen in a few other systems: Cu-Zr in the vicinity of $\text{Cu}_{10}\text{Zr}_7$,⁸ Zr_3Rh , and Zr_3Fe .⁹ Altounian *et al.*⁸ explained this behavior from the fact that the electronic density of states at the Fermi level increases upon crystal-

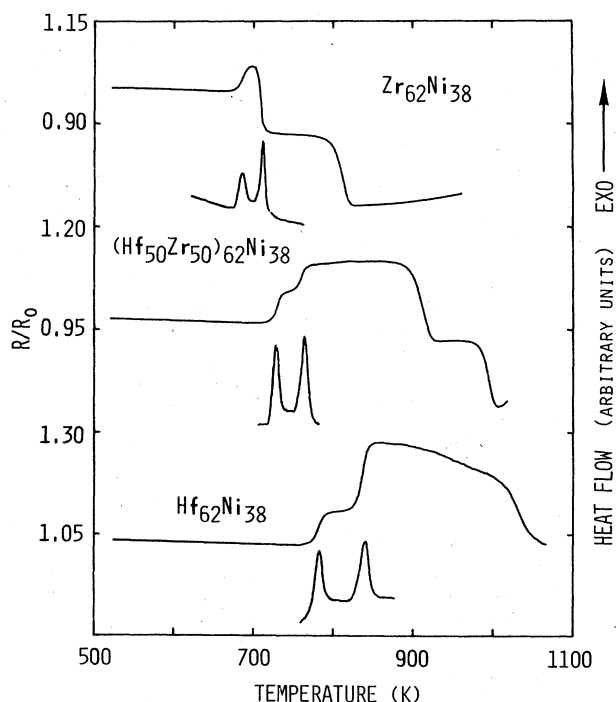


FIG. 1. Resistance and DSC traces on $\text{Zr}_{62}\text{Ni}_{38}$, $(\text{Hf}_{0.5}\text{Zr}_{0.5})_{62}\text{Ni}_{38}$, and $\text{Hf}_{62}\text{Ni}_{38}$.

TABLE I. Temperatures of the exotherms and the relative change in electrical resistance for each transition.

Alloys	T_1 (K)	Change (%)	T_2 (K)	Change (%)
$\text{Zr}_{62}\text{Ni}_{38}$	675	+6.2	700	-16.7
$(\text{Hf}_{0.5}\text{Zr}_{0.5})_{62}\text{Ni}_{38}$	730	+7.8	750	+6.5
$\text{Hf}_{62}\text{Ni}_{38}$	775	+8.5	825	+16.8

lization, which implies an increase of resistivity within the framework of the Mott s - d scattering model. Large changes in the resistivity can be observed after the second exotherm; the resistance decreases by 17% in the case of $\text{Zr}_{62}\text{Ni}_{38}$ and increases by 17% in the case of $\text{Hf}_{62}\text{Ni}_{38}$. Bragg peaks corresponding to the equilibrium phases can now be observed from high-angle x-ray scattering, contrary to samples quenched just after the first exotherm. This large difference in behavior between the Zr- and the Hf-based alloys raises some doubts as to the validity of the isomorphic substitution technique in this system. Figure 2(a) shows an enlargement of the resistivity scan below the crystallization temperature. Below 400–450 K the resistivity varies, roughly, linearly with the temperature, in agreement with the Ziman-Faber theory, which predicts linear dependence of the resistivity^{10,11} above the Debye temperature due to phonon scattering. The linear dependence is represented in the figure by the dashed line for the case of $\text{Zr}_{62}\text{Ni}_{38}$. Above 400–450 K, a departure

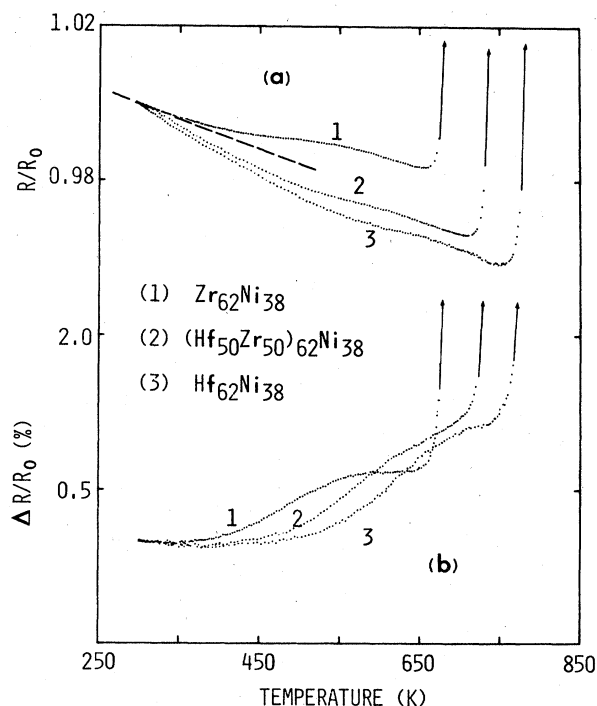


FIG. 2. (a) Enlargement of the resistance traces below the crystallization temperature. The dashed line represents the extrapolated linear dependence at low temperature. (b) Excess resistivity above the linear dependence obtained from a least-squares fit of the data at low temperature.

from the linear behavior can be observed in all three cases. Figure 2(b) represents the excess resistivity above the phonon contribution. Such behavior has been seen in a number of metallic glasses.¹²⁻¹⁴ Hillairet *et al.*¹⁵ believe that the increase in resistivity reflects an evolution towards an "equilibrium state" of chemical short-range order. They propose the existence of ordered domains, but they do not specify the exact nature of this equilibrium state.

Based on an original idea from Mott,¹⁶ Rastogi and Duwez¹⁷ suggest that microcrystalline precipitates are responsible for the additional increase in resistivity above the linear increase in amorphous Fe-P-C. Those precipitates would act as additional scattering centers for the conduction electrons in a manner similar to that found in the early stage of Guinier-Preston-zone formation in supersaturated crystalline solid solutions. In many cases, however, microcrystalline precipitates cannot be found, and all these interpretations then become speculation due to the lack of structural measurements coupled to the resistivity behavior.

Recently, we¹⁸ showed that the excess resistivity observed in $(\text{Mo}_{0.6}\text{Ru}_{0.4})_{100-x}\text{B}_x$ is correlated with the formation of domains of high and low boron concentration within the amorphous matrix. In $\text{Cu}_{50}\text{Zr}_{50}$ we showed that the anomalous resistivity behavior is due to phase separation into Cu-rich and Cu-poor zones of concentration close to $\text{Cu}_{10}\text{Zr}_7$ and CuZr_2 , respectively.¹⁹ From low-temperature specific-heat experiments, Kroeger *et al.*²⁰ observed phase separation and chemical short-

range ordering in Zr-Ni glasses between 60 and 66 at. % Zr. They have found in a 61.2 at. % Zr glass, showing no evidence of phase separation as-quenched, that annealing for 1 h at 200 °C induced phase separation into two phases of concentration near Zr_3Ni_2 and Zr_2Ni . A heat treatment as low as 150 °C for 30 min produced great changes in the volume fraction of these two phases in a 62.9 at. % Zr glass which was already phase-separated as-cast. The lowest annealing temperature at which they report phase separation (~ 150 °C or 423 K) coincides with the onset of the resistivity increase in Fig. 2(b). We then conclude that the excess resistivity observed in $(\text{Zr}_{1-x}\text{Hf}_x)_{62}\text{Ni}_{38}$ is caused by phase separation. We also see in Fig. 2(b) that Hf-based glasses are more stable against phase separation than Zr-based glasses.

In order to study the structural transformation which takes place during the first exotherm, we heat the samples to different locations within the crystallization range at a heating rate of 15 °C/min and then quench rapidly to room temperature. The solid lines in Fig. 3 represent the radial-distribution functions for as-quenched (a) $\text{Zr}_{62}\text{Ni}_{38}$, (b) $(\text{Hf}_{0.5}\text{Zr}_{0.5})_{62}\text{Ni}_{38}$, and (c) $\text{Hf}_{62}\text{Ni}_{38}$. The results are very similar to the ones reported by Wagner and Lee²¹ on $(\text{Zr}_{1-x}\text{Hf}_x)_{65}\text{Ni}_{35}$. The reduced radial-distribution function exhibits a split first peak. The first maximum at $r'_1 = 2.69$ Å decreases in height with increasing Hf content and corresponds to Ni-(Zr,Hf) neighbors. The second at $r'_1 = 3.20$ Å becomes larger in height with increasing

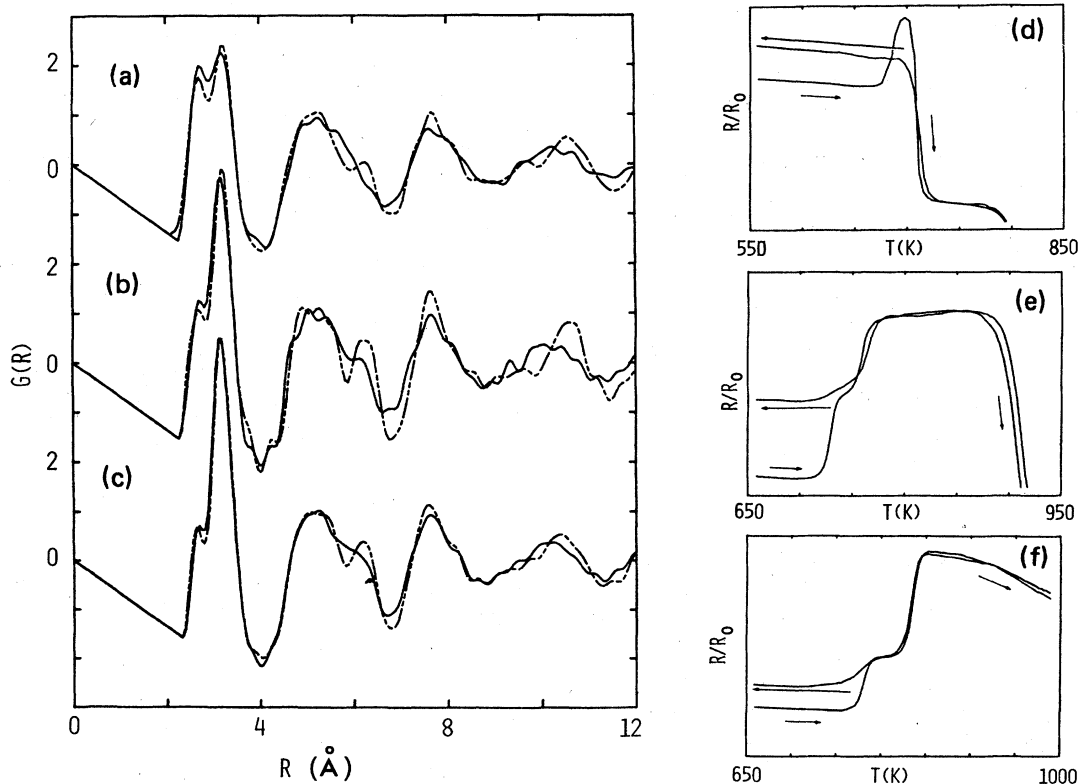


FIG. 3. Radial-distribution function before (solid lines) and after (dashed lines) the heat treatment represented in (d)–(f) for (a) $\text{Zr}_{62}\text{Ni}_{38}$, (b) $(\text{Hf}_{0.5}\text{Zr}_{0.5})_{62}\text{Ni}_{38}$, and (c) $\text{Hf}_{62}\text{Ni}_{38}$.

Hf concentration, and it corresponds to (Zr,Hf)-(Zr,Hf) neighbor pairs.

The dashed lines show the reduced radial-distribution functions after the heat treatment represented in Figs. 3(d)–3(f). For $Zr_{62}Ni_{38}$ [Fig. 3(d)] the sample was quenched just at the onset of the second exotherm (or at the onset of the resistivity drop). The height of the first peak is reduced by about 13%, which indicates a reduction in the number of unlike neighbors (Zr-Ni), and the second peak increases by about 6%, reflecting an increase in the number of Zr-Zr neighbors. $(Zr_{0.5}Hf_{0.5})_{62}Ni_{38}$ [Fig. 3(e)] was quenched between the two exotherms, or right at the maximum of the first resistivity increase. The changes in the first band are similar to the previous case (reduction of the first peak by $\sim 15\%$ and increase of the second peak by $\sim 5\%$), which strongly suggests that Hf behaves like Zr during the first phase transition. Finally, we quenched $Hf_{62}Ni_{38}$ at the onset of the first exotherm. The two subpeaks of the main band are now better resolved compared to the as-quenched sample, and the respective height of each peak remains unchanged, con-

trary to the previous cases. The shoulder at large r of the second band is also better defined and slightly more intense. This last case is typical of topological relaxation²² and does not reflect any change in the chemical short-range order. We then conclude that the increase of resistivity during the first exotherm is due to a reduction in a number or Zr-Ni neighbors and an increase in the number or Zr-Zr neighbors. In $Zr_{65}Ni_{35}$, Wagner and Lee²¹ found a Warren chemical-short-range-order parameter of -0.04 , indicating a slight preference for unlike neighbors in the first coordination shell. The following values were obtained for the coordination numbers: $N(Ni-Ni)=3.1$, $N(Ni-Zr)=8.6$, and $N(Zr-Zr)=9.2$. Roughly speaking, our results suggest that the number of Zr-Ni neighbors should decrease to around 7.4 and the number of Zr-Zr neighbors should increase to around 9.7.

This study could actually provide an interesting way to test the applicability of the Faber-Ziman theory in this amorphous alloy. The resistivity in its most general form can be written as²³

$$\rho = \beta \{ c_1 \langle |t_1|^2 a_{11} \rangle + c_2 \langle |t_2|^2 a_{22} \rangle + c_1 c_2 [\langle |t_1|^2 (1 - a_{11}) \rangle + \langle |t_2|^2 (1 - a_{22}) \rangle + \langle (t_1 t_2^* - t_1^* t_2) (a_{12} - 1) \rangle] \}. \quad (1)$$

c_1 and c_2 are the concentrations of the two constituents, t_1 and t_2 are the single-site scattering matrices, the a 's are the various partial structure factors, β depends on the average atomic volume, the electron density, and the Fermi velocity; the average $\langle f(k) \rangle$ means

$$\langle f(k) \rangle = \int_0^{2k_F} f(K) K^3 dK. \quad (2)$$

Using the isomorphic substitution technique to measure the partial structure factors before and after the first exotherm, and the t matrices for Ni (Ref. 24) and Zr (Ref. 25), we can write, in the limit of a constant prefactor,

$$\frac{\Delta \rho}{\rho_0} = \frac{\beta}{\rho_0} [c_1^2 \langle |t_1|^2 \Delta a_{11} \rangle + c_2^2 \langle |t_2|^2 \Delta a_{22} \rangle + c_1 c_2 \langle (t_1 t_2^* - t_1^* t_2) \Delta a_{12} \rangle]. \quad (3)$$

This approach is presently under investigation.

Figure 4 shows the superconducting transition in $Zr_{62}Ni_{38}$ as measured by electrical resistance changes at a temperature of 1.6 K for different applied magnetic fields. The as-quenched sample shows a very broad transition, which has been seen before in other Zr-based metallic glasses.²⁶ It was suggested that such behavior, coupled with other superconducting anomalies, such as the enhancement of H_{c2} at low temperature, may be due to spatial inhomogeneities on a scale the order of the superconducting coherence length.²⁷ Carter *et al.* proposed the existence of a distribution of electronic diffusivity $D = \frac{1}{3} v_F l$ due to variations in short-range order or to fluctuations in composition. This assumption would be in agreement with that of Kroeger *et al.*,⁵ who proposed the existence of clusters of Zr_3Ni_2 and Zr_2Ni together with unassociated atoms in the amorphous matrix. After the heat treatment beyond the first exotherm, we observe a

sharp transition characteristic of homogeneous phases, even though the heat-treated sample clearly shows two distinct phases in Fig. 5. The upper critical field, indicated by the arrows in Fig. 4, is plotted versus the temperature in Fig. 5. The anomalous linear $H_{c2}(T)$ behavior is noticeable in the as-quenched sample since curvature should be observable for the lowest measured temperatures.

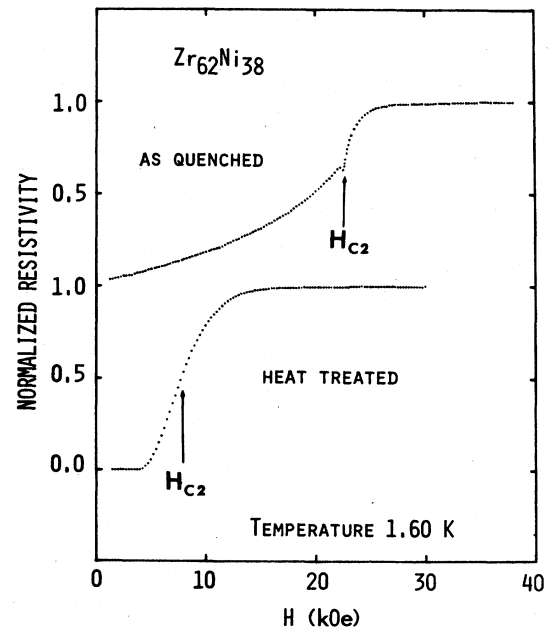


FIG. 4. Superconducting transition measured resistively for $Zr_{62}Ni_{38}$ as-quenched and heat-treated beyond the first exotherm.

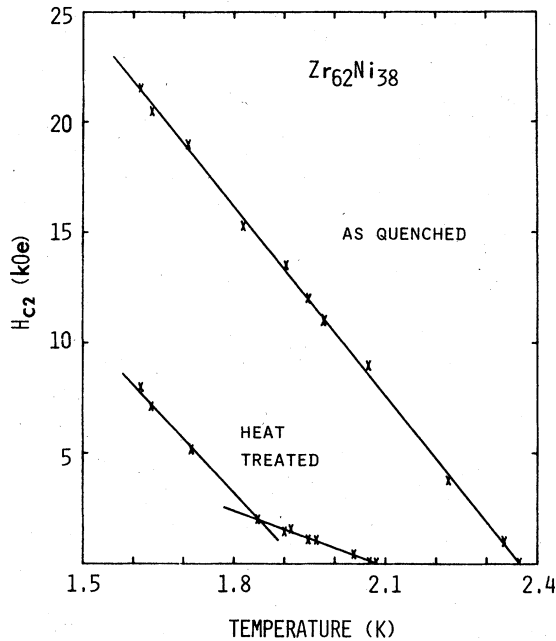


FIG. 5. Upper critical field vs temperature for $Zr_{62}Ni_{38}$ as-quenched and heat-treated beyond the first exotherm at a heating rate of $15^{\circ}C/min$.

Table II gives the T_c , critical-field gradient $dH_{c2}/dT|_{T_c}$ and the average electronic diffusivity $D = \frac{1}{3}v_F l$ (l is the average electronic mean free path and v_F is the average Fermi-velocity) for the different phases using the relation²⁸

$$\frac{dH_{c2}}{dT} \Big|_{T_c} = \frac{4k_B c}{\pi e D}, \quad (4)$$

where c is the speed of light, k_B is the Boltzmann constant, and e is the electronic charge. The T_c of the as-quenched sample is slightly lower than that reported by Kroeger *et al.*⁵ for the same composition (2.50 K). Many possible reasons can account for this discrepancy: (1) The state of relaxation of the glass. We know that T_c decreases upon free-volume relaxation, and we use melt-spun ribbons whereas Kroeger's specimens were quenched by arc hammer. (2) The difference in the measuring tech-

TABLE II. Superconductivity transitions, critical-field gradients, and average electronic diffusivities for as-quenched and heat-treated $Zr_{62}Ni_{38}$.

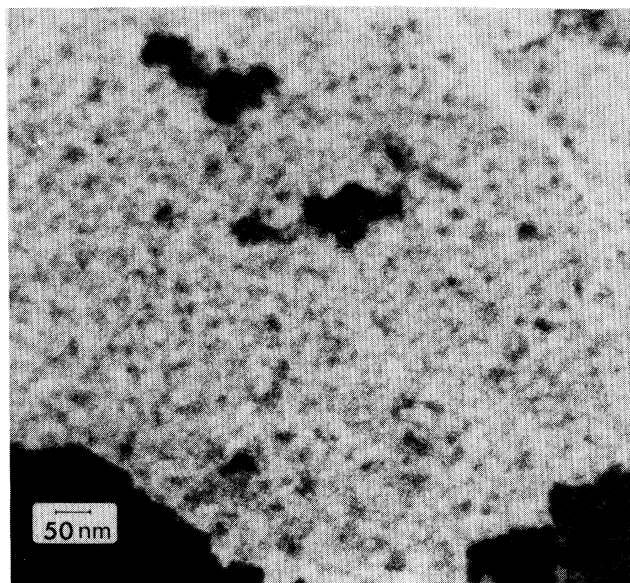
Phases	T_c (K)	$\frac{dH_{c2}}{dT} \Big _{T_c}$ (kG/K)	D (cm ² /s)
As-quenched	2.36	28.6	0.384
Heat-treated			
Phase 1	1.92	25.5	0.430
Phase 2	2.09	8.0	1.371

nique. Our result comes from the extrapolation of the H_{c2} -vs- T curve, whereas Kroeger's result comes from specific-heat measurements. (3) Finally, we cannot omit the possibility of a slight offset in the concentration of the alloy. After heat treatment, phase 1, with a T_c of 1.92 K, has almost the same critical-field gradient or average electronic diffusivity as the amorphous as-quenched sample, whereas phase 2, with a T_c of 2.09 K, has an average electronic diffusivity more than 3 times larger. We thus consider phase 1 to be the remaining amorphous state after the phase transition. From a plot of T_c versus composition⁵ we evaluated its concentration at ~ 56 at. % Zr. It is worth mentioning that this concentration corresponds to a maximum in the resistivity-versus-concentration curve for the Zr-Ni system.²⁹

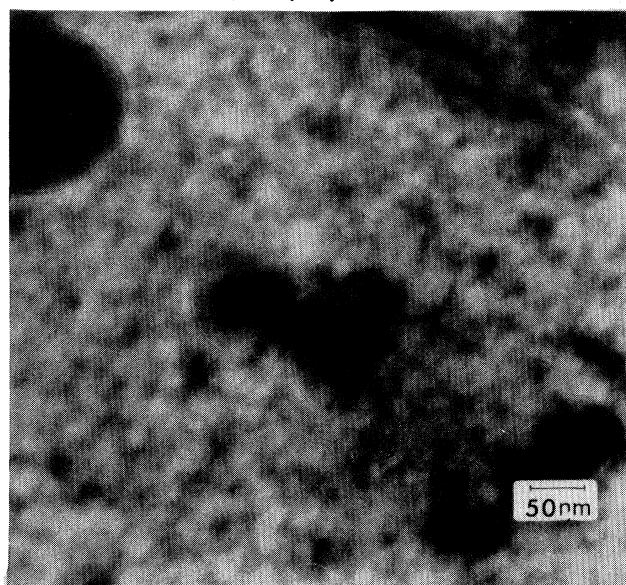
The resistivity of $Zr_{55}Ni_{45}$ is $185 \mu\Omega cm$, whereas that of the initial amorphous $Zr_{62}Ni_{38}$ is $174 \mu\Omega cm$.^{1,29} This represents an increase of 6.3%, which is exactly the jump height observed in the resistivity during the first exotherm. This correlation suggests that phase 1 dominates the transport properties at high temperature. The resistivity would seem to be unaffected by the relatively high conducting phase 2, even though phase 2 is observable at low temperature from superconducting measurements monitored by resistance changes.

Figures 6(a) and 6(b) show transmission electron micrographs for heat-treated $Zr_{62}Ni_{38}$. The micrographs show a distribution of dark speckles ranging from 10 to 30 Å in diameter. Agglomeration of these speckles produces the dark patches (average size 100–200 Å) in the micrographs. Figure 7(a) shows the electron-diffraction pattern of a selected area of Fig. 6(a) free of pits and holes. The pattern shows only a broad single halo and from it there is no evidence for phase separation or crystallization. When the area under investigation includes holes or large pits, we can detect crystals in the diffraction pattern, Fig. 7(b). This probably reflects the presence of easy-crystallization sites for heterogeneous nucleation or oxide films. Walter *et al.*³⁰ noticed oxide films at the bottom of deep pits in their thinned, transmission-electron-microscopy (TEM) samples of Zr_2Ni .

In order to investigate the local short-range order of this new phase, we introduce Fe as a probe element in the matrix and perform Mössbauer experiments. Figure 8 shows spectra of $(Zr_{62}Ni_{38})_{99.8}Fe_{0.2}$ in the as-quenched condition, heat-treated beyond the first exotherm and fully crystallized after the second. The spectra were analyzed using a least-squares fit of multiple Lorentzian lines with variable height and width. Table III gives the average quadrupole splitting corresponding to the different sites. Our results are very similar to the ones reported by Wagner *et al.*³¹ on $Zr_{95-x}Ni_xFe_5$. These authors discuss the similarities between the Mössbauer parameters of the stable crystalline phase ($\Delta E_q = 0.537$), which, as in the present case, is mainly tetragonal $Zr_2Ni(Fe)$ (CuAl₂-type structure), and the average parameters observed in amorphous Zr-Ni-Fe ($\Delta E_q = 0.608$). They suggest that the average Fe environment in the glass might be similar to that of Fe in crystalline $Zr_2Ni(Fe)$. This would be in agreement with the presence of Zr_2Ni -type associates in the amorphous state, as sug-



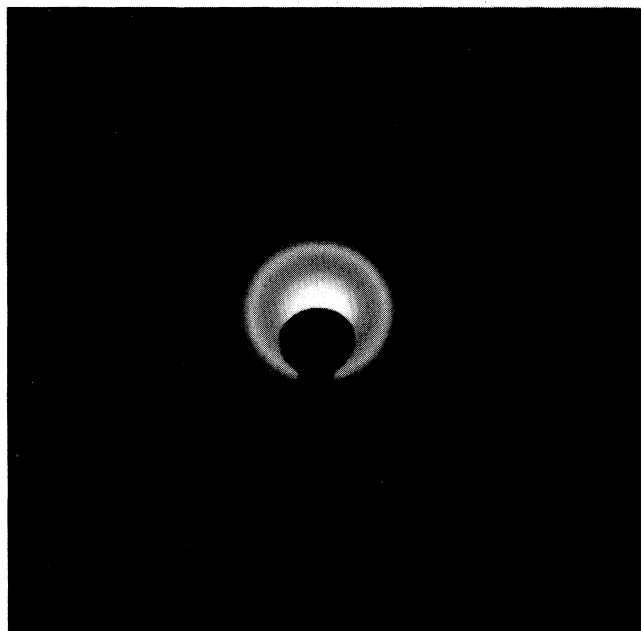
(a)



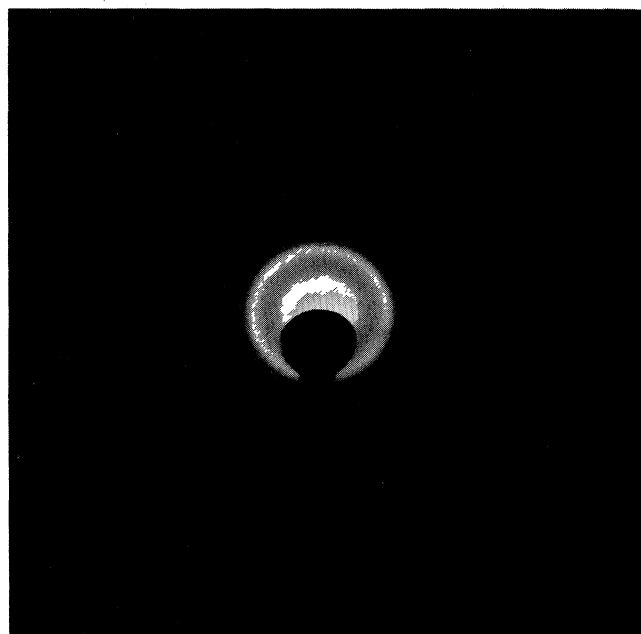
(b)

FIG. 6. (a) and (b) TEM micrographs of heat-treated $Zr_{62}Ni_{38}$.

gested by Kroeger *et al.*⁵ In this environment each Fe atom is surrounded by Zr atoms only, with the average coordination of eight Zr atoms arranged in an Archimedean antiprism capped by two Fe atoms. The Zr sites have eleven Zr and four Fe atoms as first neighbors. The heat-treated sample shows two very distinct sites. Site 1 has almost the same average quadrupole splitting as in the as-quenched sample. This site corresponds to phase 1 in Table II and represents the Ni-enriched amorphous matrix. Site 2, which must be representative of phase 2 in Table II, has a relatively large quadrupole splitting (0.931 mm/s). This value is almost identical to the one reported



(a)



(b)

FIG. 7. Diffraction pattern of heat-treated $Zr_{62}Ni_{38}$: (a) Selected area in Fig. 6 containing no pits and holes; (b) area including holes and sample edges.

by Vincze *et al.*³² for Fe in orthorhombic Zr_3Fe (Re_3B type). If Fe substitutes for Ni in the amorphous matrix and behaves in the same manner as Ni during the phase transition associated with the first exotherm, the above results would suggest the existence of a new metastable phase, orthorhombic Zr_3Ni . In this environment the Fe site has six Zr-atom first neighbors and three Fe atoms somewhat further away, while the two Zr sites have two

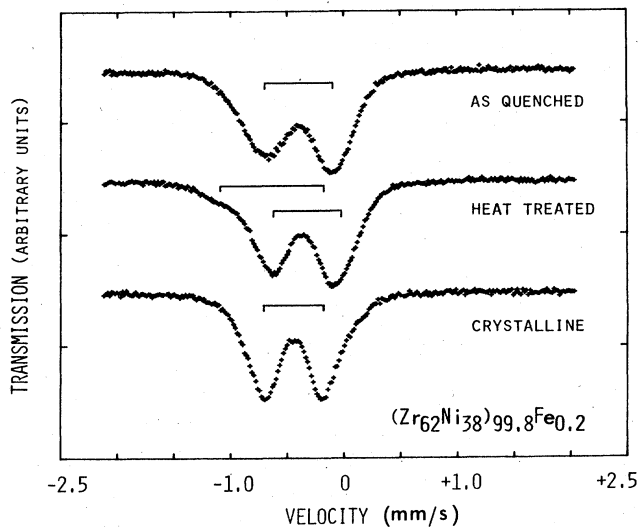


FIG. 8. Mössbauer spectra for $(\text{Zr}_{62}\text{Ni}_{38})_{99.8}\text{Fe}_{0.2}$ as-quenched, and heat-treated beyond the first exotherm, and fully crystallized after the second exotherm.

Fe and twelve Zr atoms in one case, and three Fe and eleven Zr atoms in the other case. This structure has a lower number of Zr-Ni(Fe) neighbors and a larger number of Zr-Zr neighbors than that found by Wagner and Lee²¹ for amorphous $\text{Zr}_{65}\text{Ni}_{35}$. Precipitation of an orthorhombic $\text{Zr}_3\text{Ni}(\text{Fe})$ phase would then be consistent with the reduction in the number of Zr-Ni and the increase in the number of Zr-Zr observed in the RDF after heating beyond the first exotherm.

IV. CONCLUSION

The phase transition which occurs during the first exotherm in $(\text{Zr}_{1-x}\text{Hf}_x)_{62}\text{Ni}_{38}$ metallic glasses implies pre-

TABLE III. Quadrupole splitting for different sites in $(\text{Zr}_{0.62}\text{Ni}_{0.38})_{99.8}\text{Fe}_{0.2}$ alloys.

Alloy treatment	Quadrupole splitting (mm/s)	Remarks
As-quenched	0.608	Fit to two Lorentzians
Heat-treated		
Site 1	0.615	Fit to four Lorentzians
Site 2	0.931	
Crystalline	0.537	Fit to two Lorentzians

cipitation of very small ordered clusters (10–20 Å size) which are too small to give rise to sharp rings in the diffraction pattern. The overall number of Zr-Ni neighbors decreases and the number of Zr-Zr neighbors increases. The resistivity increases because the Ni-enriched amorphous matrix that remains after precipitation has a higher electrical resistivity than the original amorphous phase, thus overcompensating for the influence of the highly conducting precipitates. Agglomeration of the clusters into zones larger than the superconducting coherence length gives rise to two distinct observable phases from the $H_c2(T)$ curve. The Mössbauer results on samples with Fe introduced as a probe element might suggest that pre-treatment of metastable, very-fine-grained microcrystalline $\text{Zr}_3\text{Ni}(\text{Fe})$ occurs during the first exotherm.

ACKNOWLEDGMENTS

We would like to thank Karl Unruh for his help with the analysis of the Mössbauer spectra. This work was supported by the U.S. Department of Energy (Project Agreement No. DE-AT03-81ER10870) under Contract No. DE-AM03-76SF00767.

*Permanent address: General Motors Research Laboratories, Warren, MI 48090.

¹Z. Altounian, Tu Guo-hua, and J. O. Strom-Olsen, *J. Appl. Phys.* **54**, 3111 (1983).

²O. Chipman, L. Jennings, and B. C. Giessen, *Bull. Am. Phys. Soc.* **23**, 467 (1978).

³K. H. J. Buschow, B. H. Verbeek, and A. G. Dirks, *J. Phys. D* **14**, 1087 (1981).

⁴Y. D. Dong, G. Gregan, and M. C. Scott, *J. Non-Cryst. Solids* **43**, 403 (1981).

⁵D. M. Kroeger, C. C. Koch, C. G. McKamey, and J. O. Scarbrough, *J. Non-Cryst. Solids* **61-62**, 937 (1983).

⁶M. Mehra, R. Schulz, and W. L. Johnson, *J. Non-Cryst. Solids*, **61-62**, 859 (1983).

⁷G. S. Cargill III, in *Solid State Physics*, edited by F. Seitz and D. Turnbull (Academic, New York, 1975), Vol. 30, p. 227; and A. Williams, Ph.D. thesis, California Institute of Technology, 1981.

⁸Z. Altounian, Tu Guo-hua, and J. O. Strom-Olsen, *J. Appl. Phys.* **53**, 7 (1982).

⁹R. Schulz (unpublished).

¹⁰P. J. Cote and L. V. Meisel, *Phys. Rev. Lett.* **39**, 102 (1977); *Phys. Rev. B* **15**, 2970 (1977); **16**, 2978 (1977).

¹¹S. R. Nagel, *Phys. Rev. B* **16**, 1694 (1977).

¹²H. S. Chen and D. Turnbull, *J. Chem. Phys.* **48**, 2560 (1968).

¹³P. L. Maitrepierre, *J. Appl. Phys.* **41**, 267 (1970).

¹⁴E. Balanzat and J. Hillairet, *J. Phys. F* **12**, 2907 (1978).

¹⁵J. Hillairet, E. Balanzat, N. Derradji, and A. Chamberod, *J. Non-Cryst. Solids* **61-62**, 781 (1984).

¹⁶N. F. Mott, *J. Inst. Metals* **60**, 267 (1937).

¹⁷P. K. Rastogi and Pol Duwez, *J. Non-Cryst. Solids* **5**, 1 (1970).

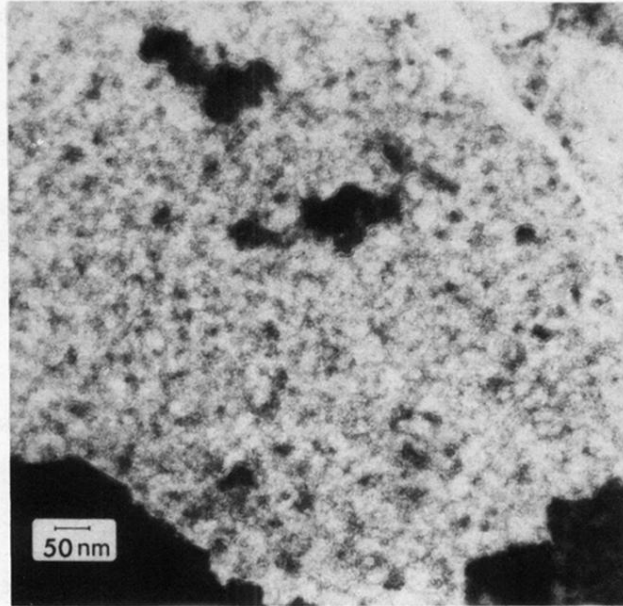
¹⁸R. Schulz, M. Mehra, and W. L. Johnson, *J. Phys. F* (to be published).

¹⁹R. Schulz, K. Samer, and W. L. Johnson, *J. Non-Cryst. Solids* **61-62**, 997 (1983).

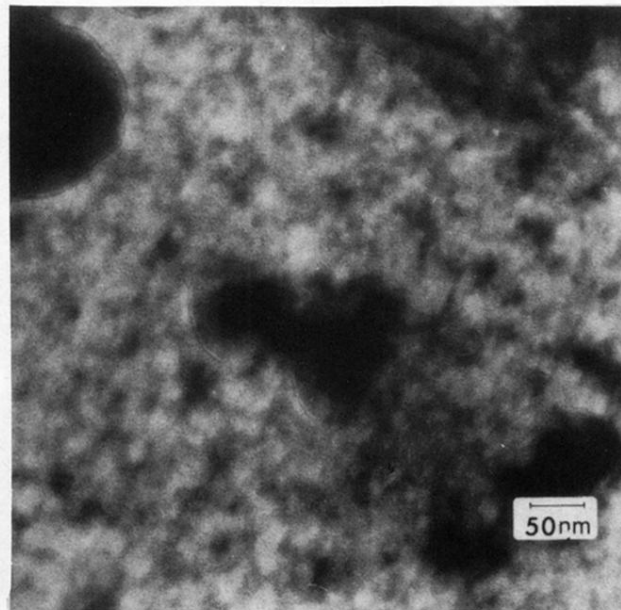
²⁰D. M. Kroeger, C. C. Koch, J. O. Scarbrough, and C. G. McKamey, *Phys. Rev. B* **29**, 1199 (1984).

²¹C. N. J. Wagner and D. Lee, *J. Phys. (Paris) Colloq.* **41**, C8-242 (1980).

- ²²D. Srolovitz, T. Egami, and V. Vitek, *Phys. Rev. B* **24**, 6936 (1981).
- ²³T. E. Faber and J. M. Ziman, *Philos. Mag.* **11**, 153 (1965).
- ²⁴O. Dreirach, R. Evans, H. J. Güntherodt, and J.-U. Kunzl, *J. Phys. F* **2**, 709 (1972).
- ²⁵Y. Waseda and H. S. Chen, *Phys. Status. Solidi A* **49**, 387 (1978).
- ²⁶M. G. Karkut and R. R. Hake, *Phys. Rev. B* **28**, 1396 (1983).
- ²⁷W. L. Carter, S. J. Poon, G. W. Hull, Jr., and T. H. Geballe, *Solid State Commun.* **39**, 41 (1981).
- ²⁸E. Helfand and N. R. Werthamer, *Phys. Rev. Lett.* **13**, 686 (1964); **147**, 288 (1966).
- ²⁹Z. Altounian, C. L. Foiles, W. B. Muir, and J. O. Strom-Olsen, *Phys. Rev. B* **27**, 1955 (1983).
- ³⁰J. L. Walter, Z. Altounian, and J. O. Strom-Olsen, *J. Non-Cryst. Solids* **61-62**, 469 (1984).
- ³¹H. G. Wagner, M. Ghafari, H. P. Klein, and U. Gonser, *J. Non-Cryst. Solids* **61-62**, 427 (1984).
- ³²I. Vincze, F. van der Woude, and M. G. Scott, *Solid State Commun.* **37**, 567 (1981).



(a)

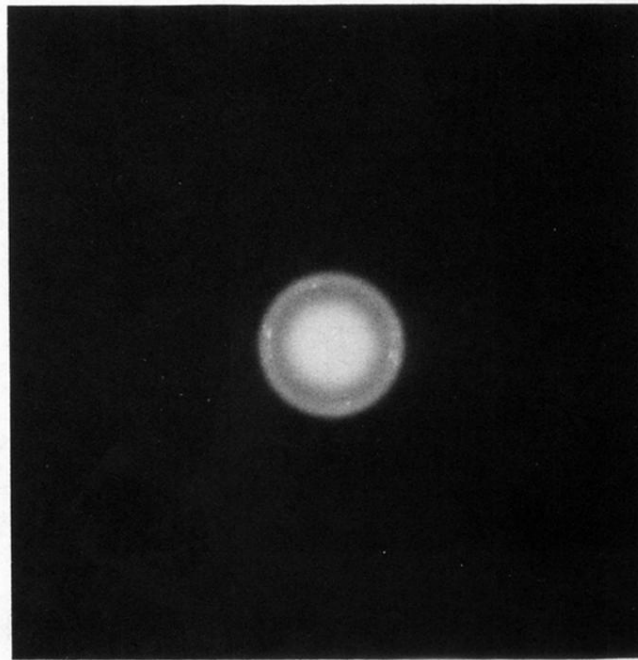


(b)

FIG. 6. (a) and (b) TEM micrographs of heat-treated $Zr_{62}Ni_{38}$.



(a)



(b)

FIG. 7. Diffraction pattern of heat-treated $Zr_{62}Ni_{38}$: (a) Selected area in Fig. 6 containing no pits and holes; (b) area including holes and sample edges.